Temperature Dependent Hall Parameter Measurements of Heterogeneous InGaAs/InP Ultrafast Transistors

James Kelly, Jing Wang, Huihua Cheng, Afesomeh Ofiare, and Chong Li

[1]University of Glasgow
{j.kelly.2, j.wang.6, h.cheng.1}@research.gla.ac.uk
{afesomeh.ofiare, chong.li}@glasgow.ac.uk

Abstract

In this paper, we present an investigation into the temperature dependence of Hall parameters, i.e., carrier density and mobility, of InGaAs/InP high electron mobility transistors fabricated in the James Watt Nanofabrication Centre at the University of Glasgow. A Lake Shore Cryotronics TTPX Probe Station setup was used to perform measurements from 77 K to 450 K under three different magnetic field strengths. The van der Pauw technique was used to determine sheet resistance and carrier density, from which carrier mobility was calculated. Two different components of the transistor structure were investigated: the channel and the cap layer. We report a channel mobility of $1.30\,\mathrm{m^2\,V^{-1}\,s^{-1}}$ at 300 K, and such, can approve the materials suitable for high frequency applications at 100 GHz and beyond.

Key Terms: Hall Effect; van der Pauw Method; InGaAs/InP; HEMTs.

1 Introduction

The sixth generation of wireless telecommunications is anticipated to arrive in the early 2030s. The key performance indicators outline an urgent necessity for materials and devices capable of operating in the terahertz frequency band [1, 2]. Simultaneously, advances in the field quantum computing technology are enabling the realisation of superconducting microwave circuits operating at milli-Kelvin temperatures [3, 4]. The progression of these two fields demands improvements in the characterisation methods of semiconductor materials under various thermal and electromagnetic conditions.

The Hall effect is a phenomenon observed in thin-film semiconductors, where the presence of a current along the length of a sample and a magnetic field penetrating the face of a sample will result in an electric force perpendicular to both the current and the field, producing a potential difference across the width of the sample called the Hall voltage [5, 6], as illustrated in Figure 1.

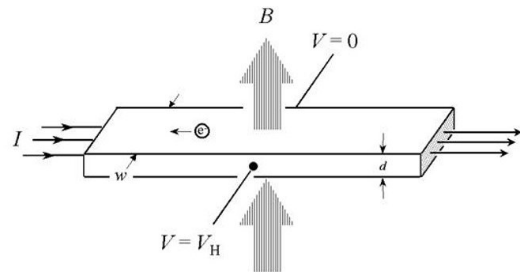

Figure 1: *A current, I, and magnetic field, B, passing through a thin semiconductor will result in a potential difference called the Hall voltage, V_H, across the width of the sample [7].*

The Hall effect is used to investigate properties of charge carriers within semiconductors – density and mobility [8, 9] – which are important parameters when characterising semiconductor devices, e.g.,

high electron mobility transistors (HEMTs). They are particularly critical for high frequency communication applications and power electronics [10, 11].

2 Van der Pauw Method

The van der Pauw four-point probing method is a technique frequently used to determine the Hall parameters of semiconductor materials [12, 13]. Figure 2 presents a selection of different arrangements for the four probe tips when performing the van der Pauw technique. The collaborators of this research paper opted to fabricate arrangement b) - the square with contacts at the corners - for simplicity.

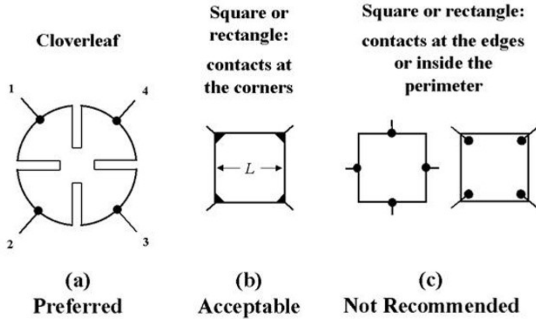

Figure 2: *Diagrams of 4 different probing configurations used in the van der Pauw method [7].*

The first step of the van der Pauw method is outlined in Figure 3, which provides diagrams of the 8 voltage, V, and current, I, bias arrangements required for calculating the sheet resistance of a sample. Subscripts 1, 2, 3 and 4 are used to refer to the four contact points. Intermediate values of resistance, R_A and R_B, can be calculated using Equations 1 and 2 respectively [7, 14].

$$R_A = \frac{\pi}{2\ln 2}\left(\frac{|V_{4,3}| + |V_{3,4}|}{|I_{1,2}| + |I_{2,1}|} + \frac{|V_{1,4}| + |V_{4,1}|}{|I_{3,2}| + |I_{2,3}|}\right) \quad (1)$$

$$R_B = \frac{\pi}{2\ln 2}\left(\frac{|V_{2,1}| + |V_{1,2}|}{|I_{4,3}| + |I_{3,4}|} + \frac{|V_{3,2}| + |V_{2,3}|}{|I_{1,4}| + |I_{4,1}|}\right) \quad (2)$$

The mean average of these gives the sheet resistance, R_S, as in Equation 3.

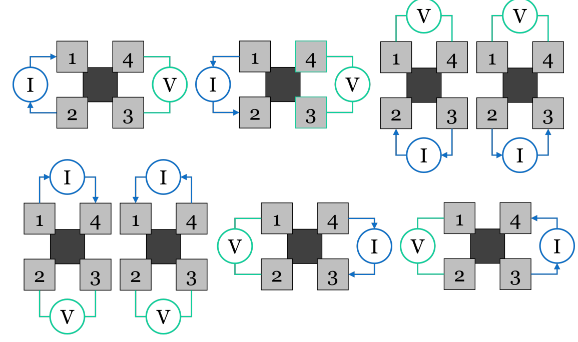

Figure 3: *The initial 8 voltage and current bias arrangements required for making sheet resistance measurements using the van der Pauw method. No magnetic field is necessary for this step [14].*

$$R_S = \frac{R_A + R_B}{2} \quad (3)$$

The second step of the van der Pauw method is shown in Figure 4. It presents two more bias arrangements, this time in the presence of a perpendicular magnetic field. These additional measurements allow for the average of the Hall voltage, V_H, over current, I, to be calculated using Equation 4.

$$\left\langle \frac{V_H}{I} \right\rangle = \frac{1}{4}\left(\frac{|V^+_{2,4}|}{|I^+_{1,3}|} + \frac{|V^+_{4,2}|}{|I^+_{3,1}|} + \frac{|V^-_{2,4}|}{|I^-_{1,3}|} + \frac{|V^-_{4,2}|}{|I^-_{3,1}|}\right) \quad (4)$$

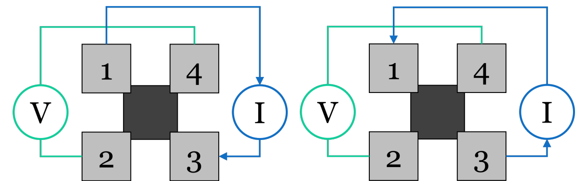

Figure 4: *The 2 voltage and current bias arrangements required (with the presence of a magnetic field) for making Hall voltage measurements using the van der Pauw method [14].*

The + and − superscripts indicate the magnetic field pointing upwards and downwards through the sample respectively. In turn, the ratio of Hall voltage to current can be used to determine sheet carrier density, n_S, using the known magnetic field strength, B, and the elemental charge, q, with Equation 5.

$$n_S = \frac{B}{q}\left\langle\frac{V_H}{I}\right\rangle^{-1} \quad (5)$$

From sheet resistance and sheet carrier density, carrier mobility, μ, can be found using Equation 6.

$$\mu = \frac{1}{q n_S R_S} \quad (6)$$

3 Device Structure & Layout

The devices measured in this research are InGaAs/InP HEMTs. Indium compounds are often utilised in high frequency wireless communications and low temperature radio astronomy applications [15, 16]. The devices were fabricated at the James Watt Nanofabrication Laboratory in Glasgow. Figure 5 presents a basic illustration of the epilayers of the samples. Two variations on the HEMT structure were fabricated: one to access the cap layer, and one to access the channel.

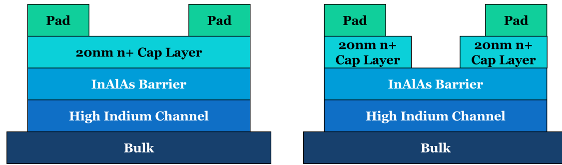

Figure 5: *Basic illustration of InGaAs/InP high electron mobility transistor structures for measuring and comparing cap layer properties (left) and channel properties (right).*

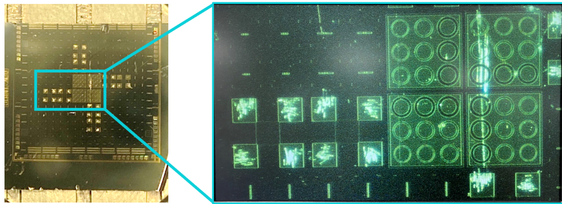

Figure 6: *Photograph of the full chip layout (left) and microscope view of the device structures (right) of InGaAs/InP high electron mobility transistors for Hall parameter measurements.*

There were 8 structures arranged on the sample in a 'windmill' arrangement. A photograph of the sample is provided in Figure 6. The diagram in Figure 7 indicates how each device was labelled: "outer" (O) or "inner" (I); and north (N), east (E), south (S) or west (W). The "outer" structures were used to measure the cap layer properties and the "inner" structures were used to measure the channel properties.

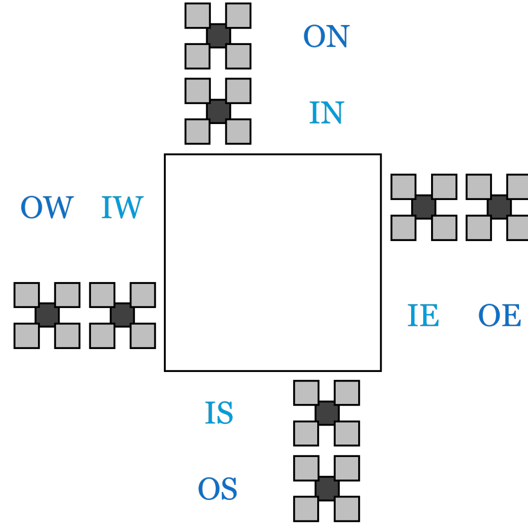

Figure 7: *Diagram of the InGaAs/InP high electron mobility transistor device and pad layouts, indicating how each structure was referenced throughout the measurements.*

4 Setup & Measurements

The characterisations were performed using a Lake Shore Cryotronics TTPX Probe Station. Temperature control was achieved with their Model 336 Temperature Controller, a Wessington Cryogenics 60 L liquid nitrogen Dewar, and an Agilent Technologies TPS-compact vacuum pump; this setup can operate within the range of 77 K to 475 K. Measurements were performed using ZN50R 10 µm tungsten probe tips connected to a Keysight B1500A Semiconductor Device Analyser. Magnetic fields were generated using the Lake Shore ring magnet kit, which enabled three different field strengths (nominally: 0.144 T; 0.177 T; and 0.190 T). Figure 8 presents a collection of photographs of the experimental setup. Measurements were taken on all 8 structures for as long

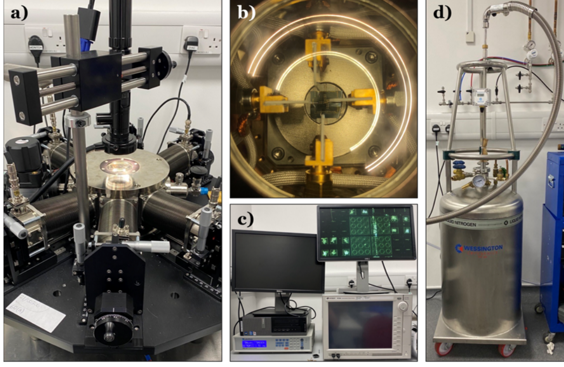

Figure 8: *a) Lake Shore Cryotronics TTPX Probe Station. b) ZN50R-10-W probe tips above the ring magnet and sample. c) Lake Shore Cryotronics Model 336 Temperature Controller and Keysight B1500A Semiconductor Device Analyser. d) Wessington Cryogenics* 60 L *liquid nitrogen Dewar.*

as possible, however, throughout this project most of the devices eventually became defective, especially after being exposed to the higher end of the temperature range. Mean average values of parameters were calculated across the "inner" and "outer" devices to account for any fabrication inconsistencies. For each arrangement given in Figures 3 and 4, a current sweep was forced from 0 mA to 1 mA, and voltage values were measured at increments of 0.2 mA. Seven temperature points were studied: 77 K; 100 K; 200 K; 300 K; 350 K; 400 K; and 450 K.

5 Results

The first investigation was to determine the effect of the magnetic field strength on the Hall parameter measurements. Table 1 provides the sheet carrier density and carrier mobility values at 300 K under each field strength, as well as the mean averages and the standard deviations of the results. These results demonstrate consistency and low deviations; this indicates that the magnetic field strength does not have a noteworthy impact on the material parameters, therefore, proceeding from this point, mean averages were also calculated across field strength. The repeatability of the values may also justify confidence in the measurement procedure.

Table 1: *Comparison of carrier density, n_S, and carrier mobility, μ, of InGaAs/InP high electron mobility transistor channel layers, measured in 3 different magnetic field strengths at* 300 K *using the van der Pauw technique. The standard deviations are given to present the consistency of the results from each field strength. Similar deviations were found for the cap layers, and at other temperature points.*

Mag. Field [T]	n_S [$10^{16}\,\mathrm{m^{-2}}$]	μ [$\mathrm{m^2\,V^{-1}\,s^{-1}}$]
0.144	2.94	1.32
0.177	2.97	1.30
0.190	3.02	1.27
Mean	**2.98**	**1.30**
σ	**0.033**	**0.021**

The most important parameter to investigate from this research is the channel mobility, which was found to be $1.30\,\mathrm{m^2\,V^{-1}\,s^{-1}}$ at 300 K. To further validate our measurements, this can be compared with simulation results and published data. The physics-based simulation tool Sentaurus was utilised as a time-saving and cost-free method for verifying the experimental results. Sentaurus employs hydrodynamic transport models for electrons, high-field saturation models for mobility, and the recombination models include Shockley–Read–Hall, Auger, and Radiative. Table 2 presents the experimental values and the simulation results for Hall mobility at different temperatures; it demonstrates that they are in excellent agreement at 300 K and 200 K. The value we report at 300 K is also in excellent agreement with measurements conducted at the James Watt Nanofabrication Centre. At 100 K, the simulation returns a significantly higher mobility than we report. Given that the simulation provides an ideal, lossless environment, this indicates that further away from room temperature our results become less accurate. This

may be due to the temperature readings being taken from the sample stage and not directly from the sample, which may have been warmer due to self-heating.

Table 2: *Comparison of experimental values and physics-based simulation results of the carrier mobility, μ, of an InGaAs/InP channel for high electron mobility transistors at different temperatures.*

Temperature [K]	$\mu_{experiment}$ [$m^2\,V^{-1}\,s^{-1}$]	$\mu_{simulation}$ [$m^2\,V^{-1}\,s^{-1}$]
300	1.30	1.295
200	1.86	1.798
100	3.13	4.239

A mobility of $1.30\,m^2\,V^{-1}\,s^{-1}$ at room temperature compares favourably against other reported indium composite channels utilised for high electron mobility transistors. This is highlighted in Table 3. From this data, we can confidently approve our materials for high frequency devices and applications.

Table 3: *Comparison of room temperature carrier mobilities, μ, of indium-based channels used in high electron mobility transistors with our channel structure $In_{0.53}Ga_{0.47}As/In_{0.80}Ga_{0.20}As/In_{0.53}Ga_{0.47}As$.*

Channel Material	μ [$m^2\,V^{-1}\,s^{-1}$]
$In_{0.23}Ga_{0.77}As$	0.46 [17]
$In_{0.8}Ga_{0.2}As$	1.15 [18]
$In_{0.53}Ga_{0.47}As/InAs/In_{0.53}Ga_{0.47}As$	1.43 [19]
$InAs/In_{0.53}Ga_{0.47}As$	1.54 [20]
This Paper	**1.30**

Figure 9 presents a plot of carrier mobility in the cap layer and the channel against temperature. It outlines a clear trend of mobility decreasing as temperature increases. This was expected, given that higher temperatures result in particles having greater thermal energies, which leads to an increase in scattering mechanisms, consequently reducing the average velocity of charge carriers.

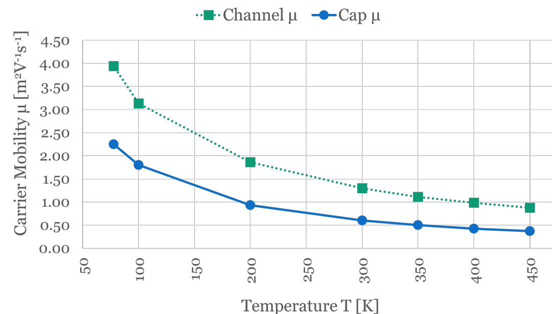

Figure 9: *Carrier mobility of cap layer and channel from InGaAs/InP high electron mobility transistors against temperature, measured using the van der Pauw method.*

6 Conclusion

An investigation was conducted into the behaviour of Hall parameters of InGaAs/InP HEMTs at varying temperatures. The van der Pauw method was used to determine sheet resistance, sheet carrier density and carrier mobility of the devices from 77 K to 450 K under 3 different magnetic field strengths. It was found that the magnetic conditions had no noteworthy impact on the semiconductor material parameters. This study found that carrier mobility decreases as temperature increases; this result was expected and can be justified by considering thermal and kinetic energy mechanisms. Relative to other similar material choices for high frequency applications, our devices performed comparably well - based on a Hall carrier mobility of $1.30\,m^2\,V^{-1}\,s^{-1}$ measured at 300 K - approving these devices suitable for such applications.

References

[1] Muhammad Waseem Akhtar et al. "The Shift to 6G Communications: Vision and Requirements". In: *Human-Centric Computing and Information Science* 10.53 (2020). DOI: 10.1186/s13673-020-00258-2.

[2] Minoru Inomata et al. “Terahertz Propagation Characteristics for 6G Mobile Communication Systems”. In: *2021 15th European Conference on Antennas and Propagation (EuCAP)*. 2021, pp. 1–5. DOI: 10.23919/EuCAP51087.2021.9411143.

[3] Morten Kjaergaard et al. “Superconducting Qubits: Current State of Play”. In: *Annual Review of Condensed Matter Physics* 11.1 (Mar. 2020), pp. 369–395. DOI: 10.1146/annurev-conmatphys-031119-050605.

[4] G Wendin. “Quantum information processing with superconducting circuits: a review”. In: *Reports on Progress in Physics* 80.10 (Sept. 2017), p. 106001. DOI: 10.1088/1361-6633/aa7e1a.

[5] Charles A. Bishop. “5 - Process Diagnostics and Coating Characteristics”. In: *Vacuum Deposition onto Webs, Films and Foils (Second Edition)*. Ed. by Charles A. Bishop. Second Edition. Oxford: William Andrew Publishing, 2011, pp. 81–114. ISBN: 978-1-4377-7867-0. DOI: https://doi.org/10.1016/B978-1-4377-7867-0.00005-2.

[6] Richard A Dunlap. “The normal Hall effect”. In: *Electrons in Solids*. 2053-2571. Morgan & Claypool Publishers, 2019, 1-1 to 1–13. ISBN: 978-1-64327-690-8. DOI: 10.1088/2053-2571/ab2f2cch1.

[7] *The Hall Effect — NIST*. https://www.nist.gov/pml/nanoscale-device-characterization-division/popular-links/hall-effect/hall-effect. Accessed: 25-10-2023. Mar. 2023.

[8] LJvd Pauw. “Method of measuring the resistivity and hall coefficient on lamellae of arbitrary shape”. In: *Philips Research Reports* 20 (1959), pp. 220–224.

[9] Changdong Chen et al. “Generalized Gated Four-Probe Method for Intrinsic Mobility Extraction With Van Der Pauw Structure”. In: *IEEE Electron Device Letters* 41.2 (2020), pp. 244–247. DOI: 10.1109/LED.2019.2959832.

[10] Zhao Jianping et al. “Technical Challenges for High-Frequency Wireless Communication”. In: *Journal of Communications and Information Networks* 1.2 (2016), pp. 19–28. DOI: 10.11959/j.issn.2096-1081.2016.033.

[11] Harsh Tataria et al. “Six Critical Challenges for 6G Wireless Systems: A Summary and Some Solutions”. In: *IEEE Vehicular Technology Magazine* 17.1 (2022), pp. 16–26. DOI: 10.1109/MVT.2021.3136506.

[12] *What is the Van-der-Pauw measurement method?* https://www.linseis.com/en/methods/van-der-pauw-measurement/. Accessed: 26-10-2023. 2023.

[13] LJvd Pauw. “A method of measuring specific resistivity and Hall effect of discs of arbitrary shape”. In: *Philips Research Reports* 13.1 (1958), pp. 1–9.

[14] *The Van Der Pauw Method of Measuring Hall Effect to Determine Mobility, Carrier Type & Concentration*. https://www.youtube.com/watch?v=bAkNC1wIlGc. Accessed: 25-10-2023. Aug. 2019.

[15] Hiroshi Hamada et al. “300-GHz-Band 120-Gb/s Wireless Front-End Based on InP-HEMT PAs and Mixers”. In: *IEEE Journal of Solid-State Circuits* 55.9 (2020), pp. 2316–2335. DOI: 10.1109/JSSC.2020.3005818.

[16] Eunjung Cha et al. “InP HEMTs for Sub-mW Cryogenic Low-Noise Amplifiers”. In: *IEEE Electron Device Letters* 41.7 (2020), pp. 1005–1008. DOI: 10.1109/LED.2020.3000071.

[17] Dagmar Gregušová et al. “GaAs Nanomembranes in the High Electron Mobility Transistor Technology”. In: *Materials* 14.13 (2021). ISSN: 1996-1944. DOI: 10.3390/ma14133461.

[18] Wan-Soo Park et al. "Extraction of effective mobility of In0.8Ga0.2As/In0.52Al0.48As quantum well high-electron-mobility transistors on InP substrate". In: *Solid-State Electronics* 197 (2022), p. 108446. ISSN: 0038-1101. DOI: https://doi.org/10.1016/j.sse.2022.108446.

[19] Yuan-Ming Chen et al. "Inverted-type InAlAs/InAs high-electron-mobility transistor with liquid phase oxidized InAlAs as gate insulator". In: *Materials (Basel)* 14.4 (Feb. 2021), p. 970. DOI: 10.3390/ma14040970.

[20] M. D. Lange et al. "InAs/InGaAs composite-channel HEMT on InP: Tailoring InGaAs thickness for performance". In: *2008 20th International Conference on Indium Phosphide and Related Materials*. 2008, pp. 1–4. DOI: 10.1109/ICIPRM.2008.4702935.